CrystEngComm

Accepted Manuscript

ROYAL SOCIETY OF CHEMISTRY

www.rsc.org/crystengcomm

Unusual hydrogen bonds pattern contributing to supramolecular assembly: Conformational study, Hirshfeld surface analysis and density functional calculations of a new steroid derivative

Alberto Ruiz,[1] Hiram Pérez,[2]* Cercis Morera-Boado,[3] Luis Almagro,[1] Cecilia C. P. da Silva,[4] Javier Ellena,[4] José M. García de la Vega,[5] Roberto Martínez-Álvarez,[6] Margarita Suárez,[1]* and Nazario Martín.[6]*

[1]Laboratorio de Síntesis Orgánica, Facultad de Química, Universidad de la Habana. 10400-La Habana, Cuba

[2]Departamento de Química Inorgánica, Facultad de Química, Universidad de La Habana, 10400-La Habana, Cuba

[3]Laboratorio de Química, Computacional y Teórica. Facultad de Química. Universidad de la Habana. 10400-La Habana, Cuba.

[4]Grupo de Cristalografía, Instituto de Física de São Carlos, Universidade de São Paulo, São Carlos, Brazil.

[5]Departamento de Química Física Aplicada. Facultad de Ciencias, Universidad Autónoma de Madrid. Spain

[6]Departamento de Química Orgánica I, Facultad de Ciencias Químicas, Universidad Complutense de Madrid, 28040 Madrid, Spain.

Corresponding authors Email: hperez@fq.uh.cu; msuarez@fq.uh.cu; nazmar@quim.ucm.es

Keywords: steroids; X-ray diffraction; hydrogen bonds; Hirshfeld surface; theoretical calculations.

Abstract

A structural and conformational study of 3β-acetoxy-17-chloro-16-formyl-5α-androstan-16-ene has been carried out by using X-ray analysis and M06-2X density functional calculations. The compound crystallizes with three independent molecules in the asymmetric unit. NBO and AIM methods were used for a better understanding of the key factors that determine the stability of this steroidal molecule, particularly the role of C-H···Cl intramolecular interaction. A detailed investigation of C-H···Cl and C-H···O intermolecular interactions, in addition to the most important van der Waals contribution, are presented by means of Hirshfeld surface analysis. The crystal packing exhibits an unusual intra- and intermolecular hydrogen bonds pattern, and show the importance of non-classical interactions for the construction of the supramolecular assembly. An excellent agreement between the theoretical and experimental data is found.

Introduction

It is well known the importance of steroids as biologically active molecules. Considering their rigid skeletons and the wide possibility of functionalization in different positions, they are excellent building scaffolds for the construction of a variety of hybrid systems.[1] Biologically active derivatives have been accomplished from natural steroids by chemical transformations of the steroid skeleton, mainly those carried out in ring D.[2,3]

Several synthetic methodologies have been utilized for the chemical functionalization of steroids. Among them, the well-know Vilsmeier–Haack reagent (formed from the reaction of

dimethylformamide with phosphorus oxychloride) has allowed in a straightforward manner the introduction of a reactive formyl group into the steroid skeleton.[4] Diverse steroids have been functionalized using this reagent yielding reactive intermediates that have been used in a further step to synthesize heterocyclic steroids with interesting biological properties such as steroidal isoxazolidinone derivatives,[5] steroidal[l7,16-*c*]pyrazoles,[6] steroidal 5´-formyl[6,5-c]pyrazoles,[7] androstenopyrazoles and androstenopyrimidines[8] as well as other interesting derivatives.[9-11]

We have recently reported the design of hybrid fullerene−steroid derivatives by reaction of pristine [60]fullerene and the respective formyl-containing steroids. By following this synthetic strategy, 3β-acetoxy-17-chloro-16-formyl-5α-androstan-16-ene (**I**), was obtained by treatment of 5α-androstan-3,17-dione and 3β-acetoxy-5α-androstan-17-one with the Vilsmeier-Haack reagent.[12]

X-ray crystallography has previously been used for the structural and conformational analysis of steroids derivatives[13-18] and the determination of the favored conformation has allowed to account for the observed pharmacological effect.

Thus, mindful of the synthetic importance of such molecules, we report herein the molecular structure of the 3β-acetoxy-17-chloro-16-formyl-5α-androstan-16-ene determined by single-crystal X-ray diffraction, and compare the results with those predicted by quantum mechanical DFT calculations. Furthermore, the Atoms in Molecules (AIM)[19,20] and Natural Bond Order (NBO)[21] analyses are used to understand the stability given by the intra- and intermolecular interactions which are responsible of the crystal packing formed from this steroidal molecule.

Results and Discussion

Structural and conformational analysis.

In the title compound **I**, which is a valuable intermediate in the synthesis of important steroid derivatives, the 3β-acetoxy group is located in an equatorial position to ring A. The remaining

functional groups in **I** are located in ring D which presents a formyl group and chlorine atom at olefinic carbons C16 and C17, respectively (See Figure 1).

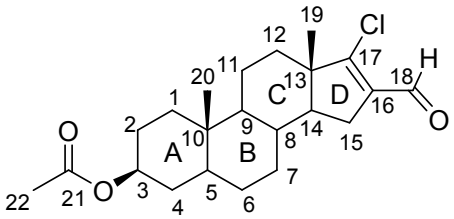

Figure 1. 3β- acetoxy-17-chloro-16-formyl-5α-androstan-16-ene (**I**)

The X-ray analysis of compound **I** reveals that it crystallizes with three independent molecules (IA, IB and IC) in the asymmetric unit, all of them with a similar conformation. The molecular structure of compound **I** with the corresponding atomic numbering scheme is shown in Figure 2.

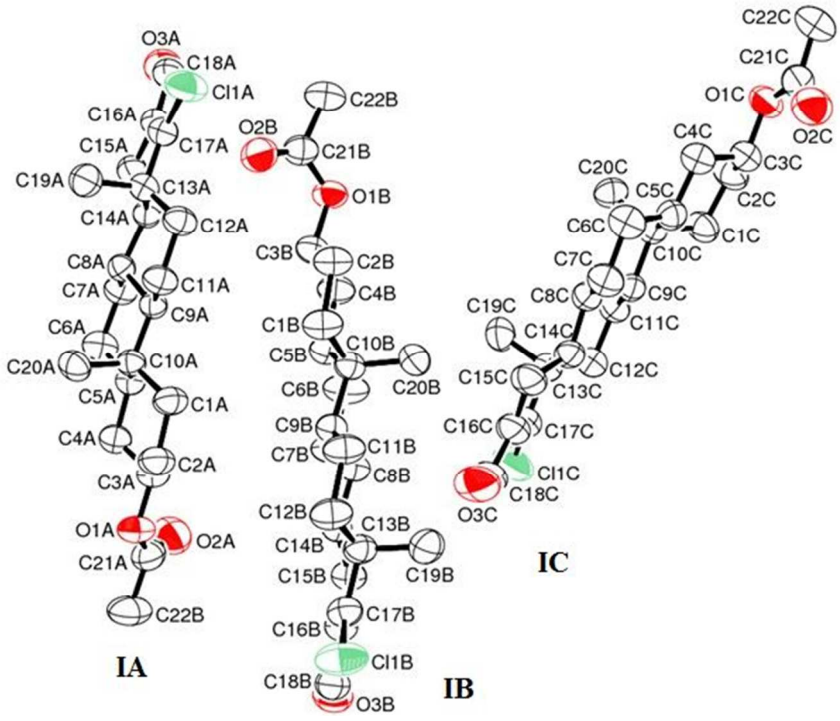

Figure 2. Molecular structure of **I** showing the atom-labeling scheme. Hydrogen atoms are omitted for clarity. The three independent molecules are shown with thermal ellipsoids drawn at the 50% probability level.

In each independent molecule, all the rings of the steroid skeleton (Figure 2) are *trans*-fused, as reflected by the average torsion angles H5-C5-C10-C20 = -178.6(2), H9-C9-C8-H8 = 177.7(2), H14-C14-C13-C19 = -172.4(2) for the *A/B*, *B/C* and *C/D* ring junctions, respectively. The acetoxy group at the C3 atom on ring *A* occupies an equatorial position. The angles between the mean plane C22/C21/O1/O2 and the normal[22] to a mean plane of the ring *A* for molecules IA, IB and IC are 63.26(7), 118.54(5) and 91.13(3)°, respectively. The six-member rings *A* and *C* have slightly flattened chair conformations, as shown by the values of their torsion angles -58.5(3) and -47.9(3)°, respectively. The saturated ring *B* adopts a chair conformation, with average puckering parameters [18]Q = 0.573(3) Å, θ = 177.7(3)° and Φ = 119(3)°. Unlike to a similar compound,[23] the ring *B* adopts a half-chair conformation The five-member ring *D* shows an envelope conformation on C14 atom, where P = 193.4(3)° and τ = 37.0(2)° are their average pseudorotation parameters.[24]

The average value of the bowing angle, the angle between the least-squares plane of ring *A* and the least-squares plane that includes the atoms of rings *B*, *C* and *D*, is 10.9(3)°. The corresponding average distance between terminal atoms C3 and C16, the length of the steroid nucleus, is 8.950 (4) Å, and the values for the pseudo-torsion angles C20–C10···C13–C19 are -4.76(2), 0.94(2) and -4.8(2)° for molecules IA, IB and IC, respectively. These values are in agreement with those found in related compounds,[13,14,25] which may be attributed to the same *A/B*, *B/C* and *C/D* ring junctions in all of these structures. The ring puckering parameters for the three independent molecules in the asymmetric unit are given in Table S1 shown in Supporting Information.

Table 1 shows selected geometrical data determined by X-ray diffraction for compound **I**, as well as those calculated by M06-2X density functional by using double and triple zeta basis set. The remaining geometrical data are collected in Tables S2, S3, and S4 shown in Supporting

Information. The bond distances and bond angles are in good agreement with the corresponding values obtained for related compounds,[26] although for the Csp3-Csp3 bond lengths extreme values for C5-C6 [1.472 (3) Å] and C9-C10 [1.567 (3) Å] were found, showing significant deviations from the average values of 1.524(4) Å for IA, IB, IC molecules. These bond lengths values are comparable with others previously reported.[27] Average C2-C3 bond length values of 1.509 (5) Å is longer than those in related steroids.[13] Moreover, there is a definite trend in the average C—O bond distance, the lengths increasing in the order C21-O2, C18-O3, 1.202(5) < C21-O1, 1.338(4) < C3-O1, 1.460(3) Å as a result of the different C-O bond character in the corresponding parts of the molecule.

There is an excellent agreement between the theoretical values of bond lengths, angles and torsion angles as compared to the three experimental structures (Table 1 and Figure S1). The lowest mean deviation (MD) values for all geometrical parameters were obtained for the highest level of calculation, e.g. with the use of the M06-2X/6-311++G(d,p) basis set. The MD values for the angles were lower than 1°, while for the torsion angles the highest MD obtained was only about 4.1°. Figure S1 (Supporting Information) shows the MD values for each geometric parameter (bond distances, bond angles and torsion angles). The calculated MD values represent the deviation of the three experimental X-ray molecules (IA, IB and IC) from the theoretically optimized structures. Figure S1 clearly shows the good agreement of both theoretical levels with the experimental X-ray structures and also that the optimized M06-2X/6-311++G(d,p) geometry presents the lowest differences with the crystallographic IB structure. This result is supported by the lowest mean deviation (MD) values obtained for the angle variables (bond and torsion angles) among the theoretically optimized geometries and the independent IB crystallographic structure.

Table 1 Selected bond distances (Å), bond angles (˚), torsion angles (˚) for the three crystallographic IA, IB and IC molecules and the two theoretically optimized structures obtained with M06-2X by using double and triple zeta basis set.

Parameters*	Experimental			Calculated	
	Molecule IA	Molecule IB	Molecule IC	[a]M06-2X/ 6-31++G(d.p)	[b]M06-2X/ 6-311++G(d.p)
Cl-C17	1.721(3)	1.720(3)	1.715(4)	1.729	1.729
O1-C21	1.334(4)	1.342(3)	1.340(4)	1.346	1.344
O1-C3	1.460 (3)	1.463(3)	1.459(3)	1.441	1.441
O2-C21	1.208(4)	1.201(3)	1.202(5)	1.208	1.202
O3-C18	1.204(5)	1.202(4)	1.210(6)	1.214	1.207
C5-C10	1.549(4)	1.545(4)	1.548(4)	1.556	1.555
C7-C8	1.523(4)	1.525(4)	1.517(4)	1.531	1.530
C13-C14	1.549(4)	1.537(4)	1.544(4)	1.546	1.545
$MD = \sum \lvert x_{exp} - x^{a}_{theor} \rvert / N$	**0.009**	**0.010**	**0.009**	In *MD* (mean deviation) expression: x = bond lengths and N= 30.	
$MD = \sum \lvert x_{exp} - x^{b}_{theor} \rvert / N$	**0.008**	**0.008**	**0.008**		
C21-O1-C3	117.5(3)	117.1(2)	117.7(3)	117.0	117.1
O1-C3-C4	111.2(2)	106.6(2)	110.7(2)	107.1	107.1
C4-C3-C2	111.9(3)	112.9(2)	112.8(3)	111.5	111.6
C13-C12-C11	109.9(2)	109.7(2)	109.7(2)	109.8	109.8
C8-C14-C15	123.2(2)	122.0(2)	122.6(2)	122.2	122.3
$MD = \sum \lvert x_{exp} - x^{a}_{theor} \rvert / N$	**0.69**	**0.55**	**0.79**	In MD expression: x = angles and N= 48.	
$MD = \sum \lvert x_{exp} - x^{b}_{theor} \rvert / N$	**0.66**	**0.52**	**0.77**		
C21-O1-C3-C2	-156.1(3)	-77.3(3)	-160(3)	-80.8	-80.9
C14-C8-C9-C11	51.3(3)	47.9(3)	51.3(3)	51.6	51.7
C7-C8-C9-C10	-55.2(3)	-58.5(3)	-55.2(3)	-55.9	-56.0
C4-C5-C10-C1	55.8(3)	56.1(3)	57.5(3)	55.0	55.1
C6-C5-C10-C9	-55.2(3)	-57.9(3)	-55(3)	-58.5	-58.6
C12-C13-C14-C8	66.3(3)	66.4(3)	65.5(3)	65.7	65.8
C17-C13-C14-C15	-34.4(2)	-35.9(2)	-35.7(3)	-35.7	-35.7
C15-C16-C18-O3	0.4(5)	2.6(5)	-0.5(7)	1.5	1.4
$MD = \sum \lvert x_{exp} - x^{a}_{theor} \rvert / N$	**4.01**	**1.66**	**4.05**	In MD expression: x = torsion angles and N= 67.	
$MD = \sum \lvert x_{exp} - x^{b}_{theor} \rvert / N$	**3.93**	**1.59**	**3.96**		

* The structure parameters are in accordance with the atom numbering scheme given in Figure 2

[a]M06-2X/6-31++G(d,p)

[b]M06-2X/6-311++G(d,p)

MD Mean deviations values calculated as $MD = \sum \lvert x_{exp} - x_{teor} \rvert / N$

Figure 3 shows two views of the packing diagram of compound **I**. In the crystal structure, each IA, IB and IC molecule is stabilized with an intramolecular C-H···Cl hydrogen bond which results in the formation of a planar pseudo five-membered ring. In addition, the molecules IB are linked by H···H contacts along the a-axes, as are the IC molecules (Figure 3a). Non-classical C-H···O and C-H···Cl intermolecular hydrogen bonds are also present between the three independent IA, IB and IC molecules (Figure 3b). The O2B and O3C atoms are involved in the formation of acceptor-bifurcated C-H···O hydrogen bonds with neighboring molecules. The C21-O1-C3-C2 torsion angle of -77.3(3)^{o} for molecule IB is shorter than the average of -158.0(3)^{o} for the molecules IA and IC (Table 1). These results can be explained by crystal packing effects, particularly, the C-H···O intermolecular hydrogen bonds formed with the O2 atom, which impose constraints to the free rotation of the acetoxy group around the O1-C3 single bond. Unlike the O2B atom forming two C-H···O hydrogen bonds (C14A-H14A···O2B, C15A-H15A···O2B) that seriously affect the free rotation of the acetoxy group, the O2A atom is only involved in the formation of C14B-H14B···O2A hydrogen bond, while the O2C atom does not present this non-classical interaction (Figure 3b). As a result, the C21-O1-C3-C2 torsion angle increases in the order: IB molecule < IA molecule < IC molecule. The optimized geometries obtained at the M06-2X with double and triple basis sets show the highest similarities with the B crystallographic molecule, with average C21-O1-C3-C2 torsion angle of -80.9°.

Cohesion in crystal structures of steroids are commonly related with the presence of C-H···O and O-H···O intra- and intermolecular hydrogen bonds as well as weak H···H van der Waals (vdW) interactions.[15-17,28-30] However, due to the presence of the chlorine atom in compound **I**, the pattern of intra- and intermolecular C-H···Cl hydrogen bonds are not typical in similar structures.[25,26] In addition, Cl···O and C-H···C intermolecular contacts are rarely found. Therefore, this prompted us to analyze the intramolecular C-H···Cl, the main intermolecular contacts, as well as the

contribution of non-classical interactions in the stability of the crystal packing of **I**.

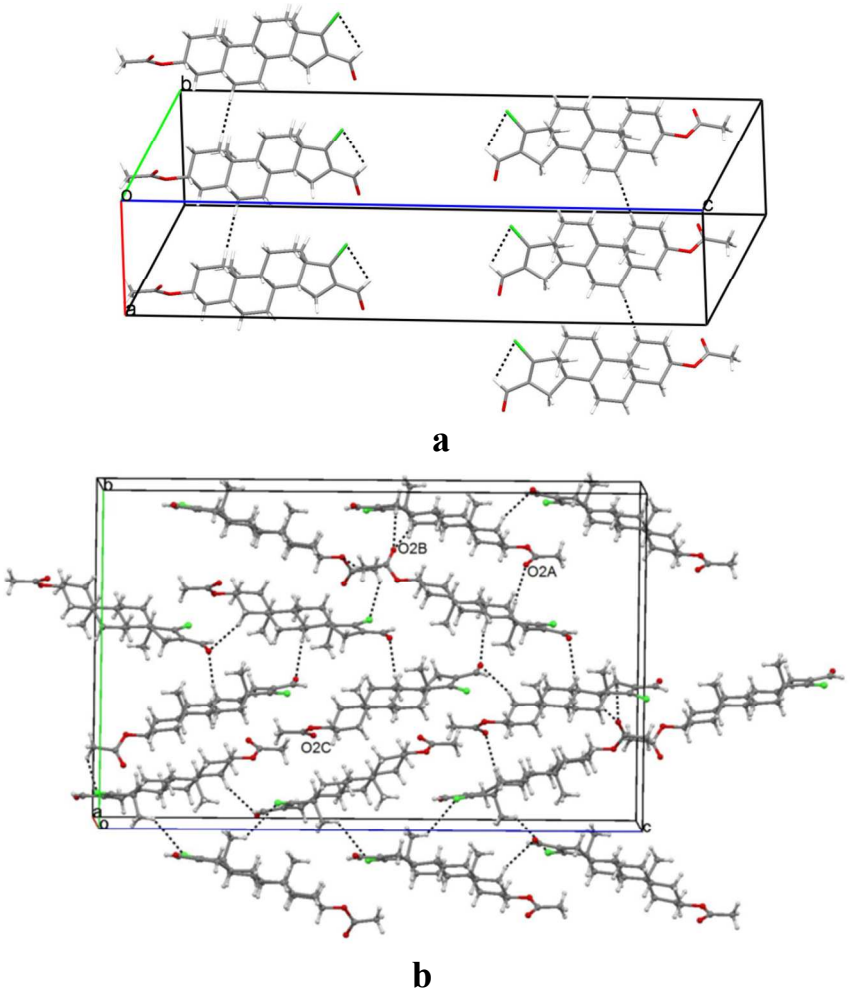

a

b

Figure 3.View of packing diagram of I showing (a) linear supramolecular chains along the a-axis mediated by H···H contacts, and C-H···Cl intramolecular hydrogen bonds. (b) C-H···O and C-H···Cl intermolecular hydrogen bonds. All the interactions are shown with dashed lines.

Analysis of the intramolecular C-H···Cl interaction

The intramolecular interaction between the chlorine atom on C17 and the formyl hydrogen atom on C18 has been studied by means of NBO and AIM methods. Figure 4 represents the potential energy curve as a function of the C17-C16-C18-H torsion angle in a partial moiety of **I**. A total of two minima were located from the potential energy curve. The global minimum was observed at 0° and 360° (chlorine and hydrogen atoms in syn disposition), while the other

minimum at 180° (chlorine and hydrogen atoms in anti-disposition) is 3.7 kcal/mol higher in energy than the global minima. The two maxima obtained at 90° and 270° were 8.5 and 8.4 kcal/mol higher in energy than the global minimum, respectively. These geometries represent transition states with only one imaginary frequency. The energy barrier is close to 8.5 kcal/mol, and the transition state in 90° proceeds to the 180° energy local minimum.

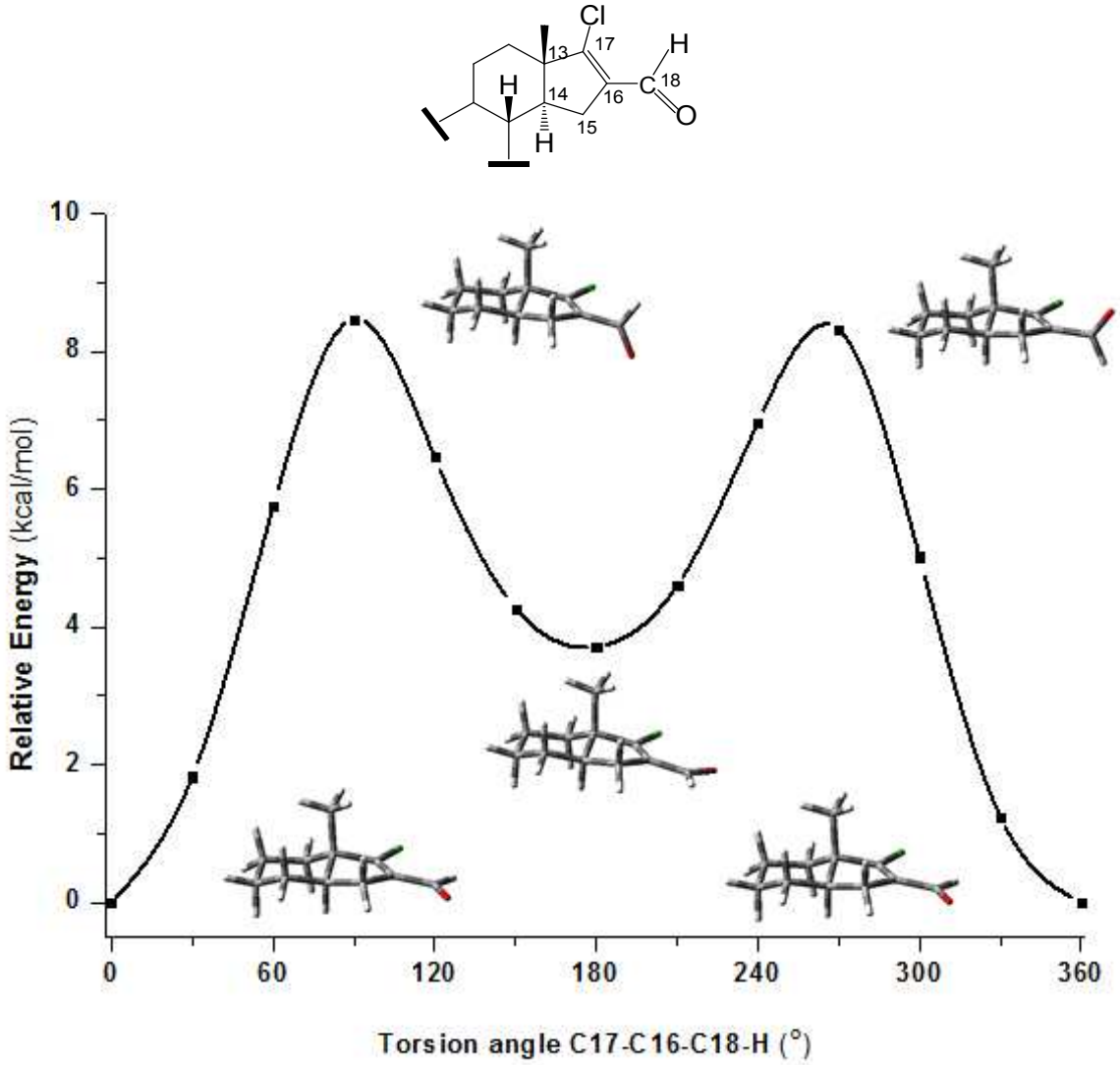

Figure 4. Potential energy curve of the model of compound **I** by rotating the C17-C16-C18-H torsion angle from 0° to 360° at the M06-2X/6-31++G(g,p) level of calculation.

The entire geometry of compound **I** was optimized for particular constrained torsion angles, C17-C16-C18-H, of 0°, 90° and 180°. As in the case of the small model (Figure 4), the structure

obtained at 90° corresponds to a transition state with a relative energy of 8.6 kcal/mol respect to the global minimum energy (0°). The local minimum energy geometry with C17-C16-C18-H torsion angle value of 180° was 3.8 kcal/mol higher in energy than the global minimum energy structure. Figure 5 shows the two minima and transition state energy structures of compound **I** after constrained optimization at the M06-2X/6-31++G(d,p) level of calculation was accomplished.

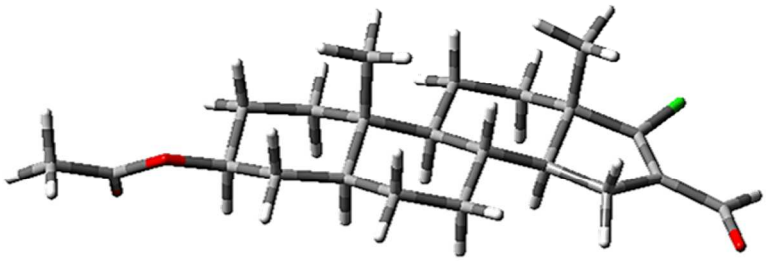

E (hartrees) = -1542.4740851, C17-C16-C18-H = 0°

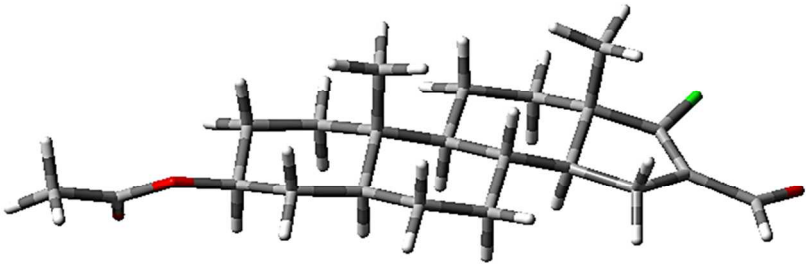

E (hartrees) = -1542.4680505, C17-C16-C18-H = 180°

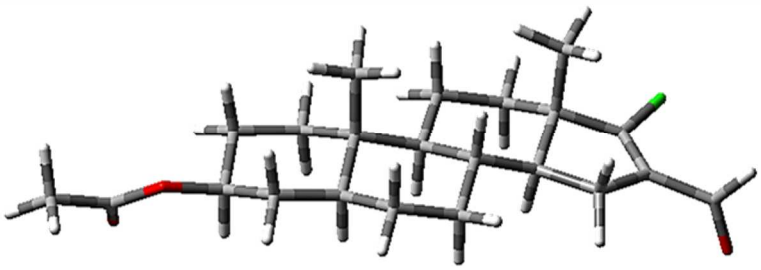

E (hartrees)= -1542.460459, C17-C16-C18-H = 90°

Figure 5. Minima energy (0°, 180°) and transition state (90°) optimized geometries at the M06-2X/6-31++G(d,p) level of theory.

To understand the difference in stabilities between these conformers, a natural bond orbital analysis NBO[21] to the geometries of compound **I** with C17-C16-C18-H torsion angles of 0°, 90°

and 180° (Figure 5) at the M06-2X/6-31++G(d,p) level of theory was performed. Three types of stabilizing contributions affect the stability of the different conformers of compound **I** (Figure 5). The $\pi_{C=C}$-$\pi^*_{C=O}$ and $\pi_{C=O}$-$\pi^*_{C=C}$ are related with delocalization of the C=C double bond in the ring *D* and the C=O bond of the formyl group attached to C16, and the third interaction is due to the presence of the C-H···Cl intramolecular contact. An analysis of the perturbative second order energies $\Delta E^{(2)}$ allows to understand the energetic stabilization given by a particular interaction between a filled donor Lewis-type NBO orbital and an acceptor non-Lewis NBO orbital.[31,32] The $\Delta E^{(2)}$ energy values of the $\pi_{C=C}$-$\pi^*_{C=O}$ interaction for 0°, 90° and 180° configurations are 22.5, 0 and 21.8 kcal/mol, respectively. As expected, when the C17-C16-C18-H torsion angle value is 90° the $\pi_{C=C}$ and $\pi^*_{C=O}$ orbitals are orthogonal, and therefore they do not interact each other, as revealed by the absence of this stabilizing $\pi_{C=C}$-$\pi^*_{C=O}$ interaction. The interaction of both π orbitals for the conformers with torsion angle values of 0° and 180° is favored, and therefore $\Delta E^{(2)}$ show the highest values for these two geometries. The $\pi_{C=C}$-$\pi^*_{C=O}$ interaction of the global minimum (0°) is only 0.7 kcal/mol more stable than in the configuration with torsion angle of 180°. As the $\pi_{C=C}$ and $\pi^*_{C=O}$ orbitals lie closer in energy, they present a stronger interaction than the $\pi_{C=O}$ and $\pi^*_{C=C}$ orbitals. The $\Delta E^{(2)}$ energy of the $\pi_{C=O}$-$\pi^*_{C=C}$ interaction show the highest values for the 0° (7.3 kcal/mol) and the 180° (6.3 kcal/mol) conformers, while for 90° was 0 kcal/mol. Then, as for $\pi_{C=C}$-$\pi^*_{C=O}$, the $\pi_{C=O}$-$\pi^*_{C=C}$ interaction stabilizes the 0° (hydrogen and chlorine atoms in syn disposition) conformer in 1 kcal/mol respect to the 180° conformation with the oxygen and chlorine atoms in syn disposition. NBO analysis of $\pi_{C=C}$-$\pi^*_{C=O}$ and $\pi_{C=O}$-$\pi^*_{C=C}$ interactions agrees well with the general trend that vicinal hyperconjugation produced among C=C and C=O is increased for antiperiplanar conformations, as is the case of the 0° conformer.[33]

The other stabilizing contribution observed in the global minimum energy structure is the formation of an intramolecular C-H···Cl interaction, which in addition to the stabilization given by the $\pi_{C=C}$-$\pi^*_{C=O}$ and $\pi_{C=O}$-$\pi^*_{C=C}$ interactions could be the cause of its highest stability. As expected, the $n^{(\pi)}_{Cl}$-σ^*_{C18-H} interaction is observed only in the global minimum energy geometry (0°). This donor NBO orbital of the chlorine atom is a p-rich π-type lone pair $n^{(\pi)}$, with a 99.98 % p-character and perpendicular to the bond axis, while the anti-bonding acceptor NBO orbital (σ^*_{C18-H}) shows the carbon atom in an $sp^{2.07}$ hybrid with 67.4 % and 32.6 % of p and s character, respectively, which shows a typical sp^2 hybridization. The presence of this NBO interaction indicates the existence of C-H···Cl intramolecular contact, exhibiting a small second order perturbative energy ($\Delta E^{(2)}$) of 0.5 kcal/mol at the M06-2X/6-31++G(d,p) level of theory. The ν_{C-H} values as a result of the C-H···Cl contact formation are blue-shifted although no significant hybridization changes are observed[34] (See Table S5, Supporting Information.)

The NBO analysis, based on the stabilizing interactions $\pi_{C=C}$-$\pi^*_{C=O}$, $\pi_{C=O}$-$\pi^*_{C=C}$ and $n^{(\pi)}_{Cl}$-σ^*_{C18-H} shows a small difference in stabilization energy that favors the global minimum energy (0°) respect to the 180° conformation. Then, the energy differences obtained in the torsion angle profile between both minima conformers are not mainly caused by these NBO interactions, but also to the existent Pauli repulsion between the oxygen and chlorine atoms oriented in a syn disposition for the local minimum geometry (180°). Figure 6 shows a contour map of the electron localization function (ELF),[35] as obtained at the M06-2X/6-31++G(d,p) level of theory. As can be seen, for the 180° conformation, the electronic density cloud of both chlorine and oxygen atoms are perturbed respect to the syn H···Cl conformer (0°). Therefore, the closed shell repulsion between chlorine and oxygen atoms in the 180° conformer possesses an important role in the destabilization of this conformation. Overall, the effect of the main stabilizing conjugative NBO interaction, $\pi_{C=C}$-$\pi^*_{C=O}$ (absent in the 90° conformer), with the destabilizing Pauli repulsion

presented only in the 180° minimum are responsible for the asymmetric shape of the double well potential.

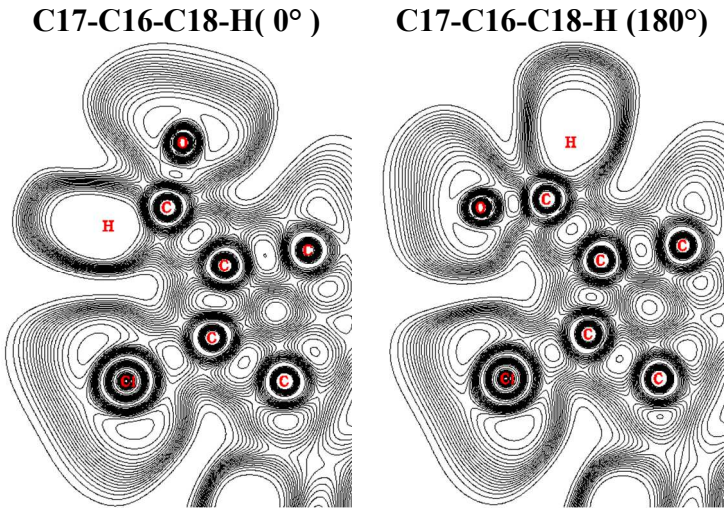

Figure 6. Contour line map of the Electron Localization Function (ELF) at the M06-2X/6-31++G(d,p) level of theory for the global (0°) and local (180°) minima energy geometries.

The AIM theory has been used in several studies to describe the topology of intra- and intermolecular interactions and to classify them in covalent and non-covalent interactions.[36-39]

Table 2 shows the experimental intra- and intermolecular hydrogen bond geometries of compound **I** as determined by single-crystal X-ray analysis. Also, the theoretical intramolecular hydrogen bond geometries as obtained by M06-2X with 6-31++G(d,p) and 6-311++G(d,p) basis sets are presented, being all intramolecular hydrogen bond parameters very close to experimental X-ray data. The *r*(molecule Exp/Theor) ratio values were greater than 0.92 for the three independent molecules, being the lowest difference for the IB molecule at the M06-2X/6-311++G(d,p) level of theory.

Table 2 Hydrogen-bond geometry for **I** [d(Å).and ∠(°)].

D–H···A	d(D–H)	d(D····A)	d(H····A)	∠(D–H····A)
C18A-H18A···Cl1A	1.025	3.215(5)	2.768(4)	106.6(2)
C18B-H18B···Cl1B	1.052	3.231(4)	2.794(1)	105.0(2)
C18C-H18C···Cl1C	1.038	3.207(6)	2.727(1)	108.0(3)
C15A-H15A···O2B^{i}	0.97	3.177(4)	2.508(2)	126.1(2)
C14A-H14A···O2B^{i}	0.98	3.344(3)	2.639(2)	129.1(1)
C14B-H14B···O2A^{ii}	0.98	3.656(4)	2.687(3)	123.6(1)
C22C-H22I···O1A^{iii}	0.96	3.623(5)	2.756(2)	150.8(2)
C19A-H19B···Cl1B^{iv}	0.96	3.998(3)	3.255(1)	151.9(2)
C22B-H22D···Cl1A^{v}	0.96	3.784(4)	2.980(1)	142.2(2)
C12C-H12C···C21C^{vi}	0.97	3.797(4)	2.840(4)	169.2(2)
C18A-H18A···Cl1^{a}	1.106	3.255	2.853	101.3
C18A-H18A···Cl1^{b}	1.104	3.251	2.845	101.5
r(Molecule IA Exp/Theor)	0.9267/0.9284	0.9877/ 0.9889	0.9702/0.9729	1.0523/ 1.0502
r(Molecule IB Exp/Theor)	0.9511/0.9529	0.9926/0.9938	0.9793/0.9821	1.0365/1.0344
r(Molecule IC Exp/Theor)	0.9385/0.9402	0.9852/0.9864	0.9558/0.9585	1.0661/1.0640

Symmetrycodes: (i) 1+x,y,z; (ii) 1-x,½+y,½-z; (iii) 2-x,½+y,½-z; (iv) –x,-½+y,½-z; (v) ½+x,½-y,-z; (vi) ½+x,1.5-y,-z

Value taken from optimized structure at [a]M06-2X/6-31++G(d.p) and [b]M06-2X/6-311++G(d.p).

r (molecule Exp-Theor)-ratio of the experimental crystallographic geometry with both theoretical method:M06-2X/6-31++G(d,p)/M06-2X/6-311++G(d,p))

Surprisingly, when the AIM method was applied to the optimized geometry of compound **I** with d(H···Cl) = 2.845 Å no *bond critical point* (*bcp*) could be identified along the path connecting hydrogen and chlorine atoms. Hence, the AIM analysis was repeated for the three independent crystallographic structures A, B and C with d(H···Cl) distances shorter than the one previously obtained (e.g. d(H···Cl) = 2.768 Å; 2.794 Å and 2.727 Å) for A, B and C, respectively (See Table 2). As for the optimized geometry, no critical points with the correct (3;-1) topology were observed between the acceptor and the hydrogen atom, indicating the absence of this intramolecular interaction. Then, the effect of a decrease in the d(H···Cl) distance by choosing a model of compound **I** with a fixed d(H···Cl) distance of 2.650 Å was studied. Figure 7 shows the topology of the Laplacian of the electron density ($\nabla^2\rho(bcp)$) of both models.

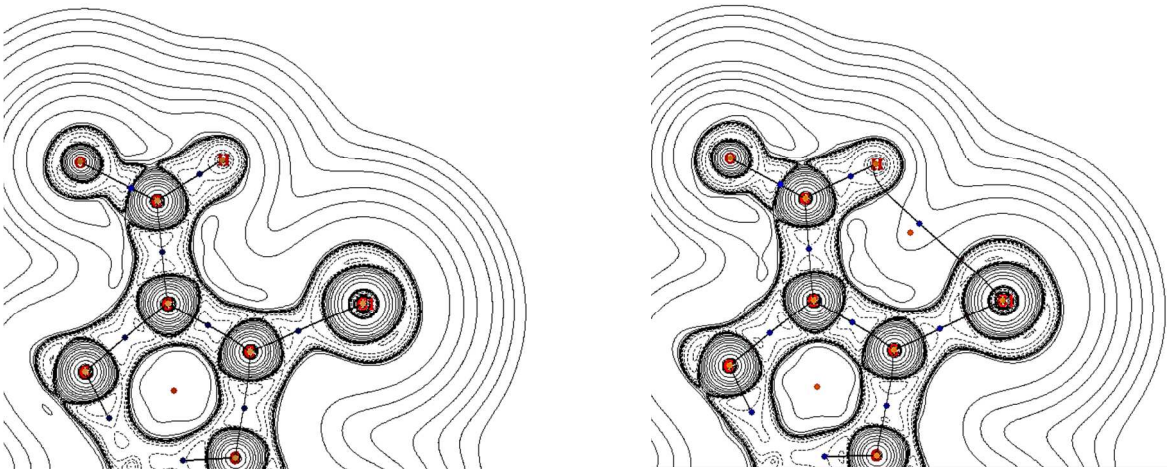

(**a**) d(H···Cl)=2.845 Å (**b**) d(H···Cl)=2.650 Å

Figure 7. Contour line map of the Laplacian of ρ of ring D with C17-Cl and C16-CHO for (a) optimized M06-2X/6-311++G(d,p) model geometry with d(H···Cl)=2.845 Å and (b) optimized M06-2X/6-311++G(d,p) model geometry with d(H···Cl)=2.650 Å. (Blue circles represent bond critical points (3;-1), yellow circles represents ring critical points (3;+1).

From Figure 7b can be clearly observed the presence of the *bcp* between hydrogen and chlorine atoms when the d(H···Cl) distance decrease to 2.650 Å. The absence of the bond path in Figure 7a is motivated by the small $d_{bcp\text{-}rcp}$ distance of 0.189 Å between the *bcp* and the *ring critical point (rcp)* of topology (3+1). When these two critical points becomes closer than in Figure 7b, they coalesce and annihilate each other, giving as a result a change in the topology of the system with the subsequent disappearance of both critical points and of the bond path connecting both atoms.[40,41] Although in the optimized M06-2X/6-311++G(d,p) geometry of compound **I** and in the crystallographic independent structures A, B and C, no bond path was obtained for this intramolecular interaction, the line plot map of the Laplacian of the density for the optimized geometry with d(H···Cl) = 2.845 Å is very similar to the model with d(H···Cl) = 2.650 Å (Figure 7a,b), where the same topology pattern can be observed between both hydrogen and chlorine atoms. The similarity of both topology patterns clearly indicates the presence of this C-H···Cl

intramolecular interaction in the optimized structure of compound **I**, as well as in the crystallographic independent IA, IB and IC molecules. The existence of this intramolecular contact was first evidenced by the presence of the $n^{(\pi)}_{Cl}$-$\sigma^*_{C18\text{-}H}$ NBO´s interaction with a small second order perturbative energy contribution. The absence of the bond path in this case does not point toward the non-existence of this intramolecular interaction, but that the system is in a particular geometry where these two critical points annihilate each other.

In order to classify the C-H···Cl intramolecular interaction, the topological parameters (ρ and $\nabla^2\rho(bcp)$) of the intramolecular bond critical point for the model compound with d(H···Cl)=2.650 Å were obtained. According to Bader,[42] Ponmalai[43] and Popelier,[44] the electron density and its Laplacian at the bond critical point must be in the range 0.002-0.035 a.u. and 0.014-0.139 a.u., respectively, to be considered as closed-shell interactions. For van der Waals (vdW) interactions, the ρ(bcp) tends to be smaller than for hydrogen bonded closed-shell type interactions, e.g. 0.002-0.009 a.u.[45] For the model compound, Figure 7b, the ρ(bcp) and $\nabla^2\rho(bcp)$ values for the intramolecular CH···Cl interaction are 0.0119 and 0.0498 a.u. respectively, which is properly within the range to be classified as a weak hydrogen bond interaction.

According to geometrical parameters, the C-H···Cl intramolecular interaction has been accepted as a very weak hydrogen bond, in the limit of vdW interactions.[46] The global minimum obtained at the M06-2X/6-311++G(d,p) level of theory with d(H···Cl) = 2.845 Å shows medium range C-H···Cl contacts, defined for *d*(H···Cl) in the range of 2.6-3.0 Å.[47] In addition, the three independent molecules and both theoretically optimized geometries for **I** with double-zeta and triple-zeta basis sets, show a medium range C-H···Cl hydrogen bond interaction[46] (Table 2).

Analysis of the intermolecular interactions

The main intermolecular interactions presented in **I** were analyzed using the Hirshfeld surface[48,49] and the corresponding two-dimensional fingerprint plots.[50,51] In previous work we used this methodology that allowed us to understand the role of hydrogen bonds in the molecular conformation of a steroid derivative and acylthioureas.[52,53]

Figure 8 shows two views of the Hirshfeld surface 3D map for molecule IA of compound **I**, which have been color coded. Using the d_{norm} (normalized contact distance) surface and the breakdown of fingerprint plots information it is possible to highlight graphically those regions of the surface involved in a specific type of intermolecular contact.[54] The surfaces are shown as transparent to allow visualization of the molecule. The red regions in Figure 8a and Figure 8b indicate H···O and H···Cl intermolecular contacts, respectively. The small extent of area and light color of this feature on the surface in Figures 8a and 8b indicates that H22I···O1A and H22D···Cl1A contacts are weaker and longer than the other hydrogen bonds.

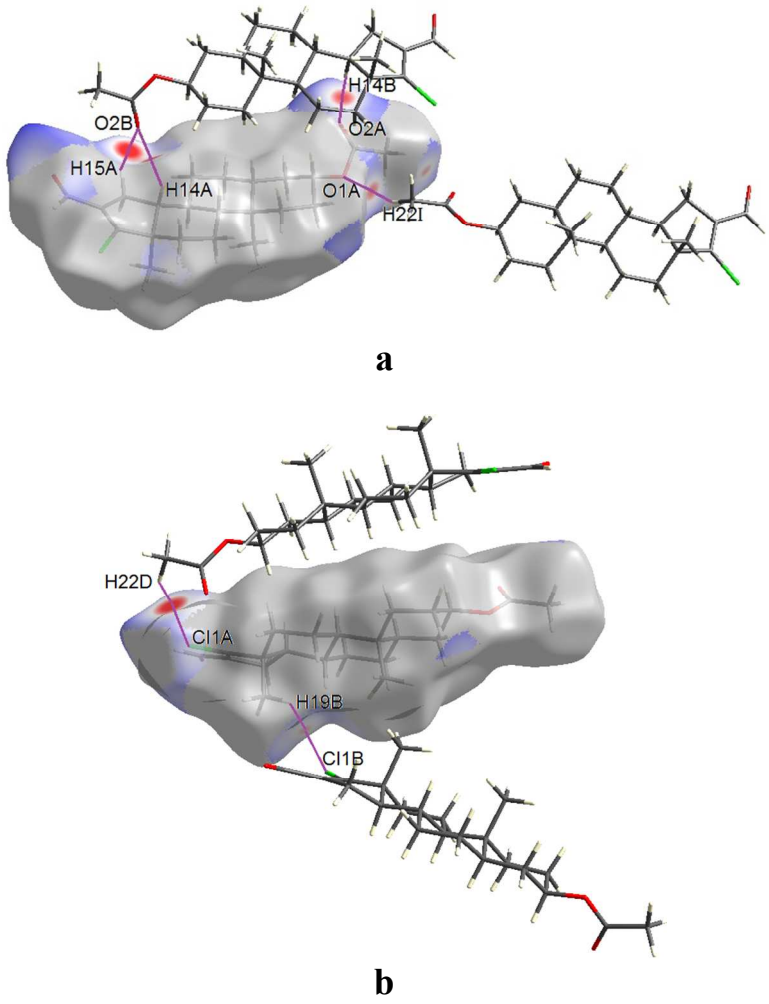

Figure 8. Views of the Hirshfeld surface for molecule IA of **I** mapped with d_{norm} property showing: (a) H···O (b) H···Cl intermolecular contacts.

Figure 9 illustrates the decomposing of fingerprint plot of molecule IA of **I** in crystal lattice, highlighting separately the H···H, H···O, H···Cl and H···C intermolecular contacts. To provide context, the outline of the full fingerprint is shown in gray, and the blue area shows the separate contact. Figure 9a isolates very short H···H contacts and shows spikes centred near a (de + di) sum of 2.23 Å [H1E···H6E^{i} = 2.31Å, H11H···H3C^{ii} = 2.32 Å; symmetry codes: (i) -1+x, y,z; (ii) ½+x,1.5-y,-z]. Figure 9b isolates H···O interactions and shows spikes centered a (de+di) sum with the range of 2.42-2.49 Å [H15A···O2B^{i} = 2.508(2) Å, H22I···O1A^{ii}= 2.756(2) Å; symmetry codes: (i) 1+x, y,z; (ii) 2-x,½+y,½-z]. These results indicate strong H···O intermolecular contacts.[55]

Figure 9c isolates H···Cl contacts and shows spikes centred a (de+di) sum with the range of 2.86-3.14 Å [H22D···Cl1A^{i} = 2.980(1) Å, H22I···Cl1A^{ii} = 3.255(1) Å; symmetry codes: (i) ½+x, ½-y,-z; (ii) -x,-½+y,½-z]. Values in brackets correspond to the experimental X-ray data. Figure 9d isolates H···C intermolecular contacts and exhibits spikes centred a (de+di) sum with the range of 2.83-2.93 Å. These results indicate moderate H···Cl and weak H···C intermolecular hydrogen bonds, respectively.[55]

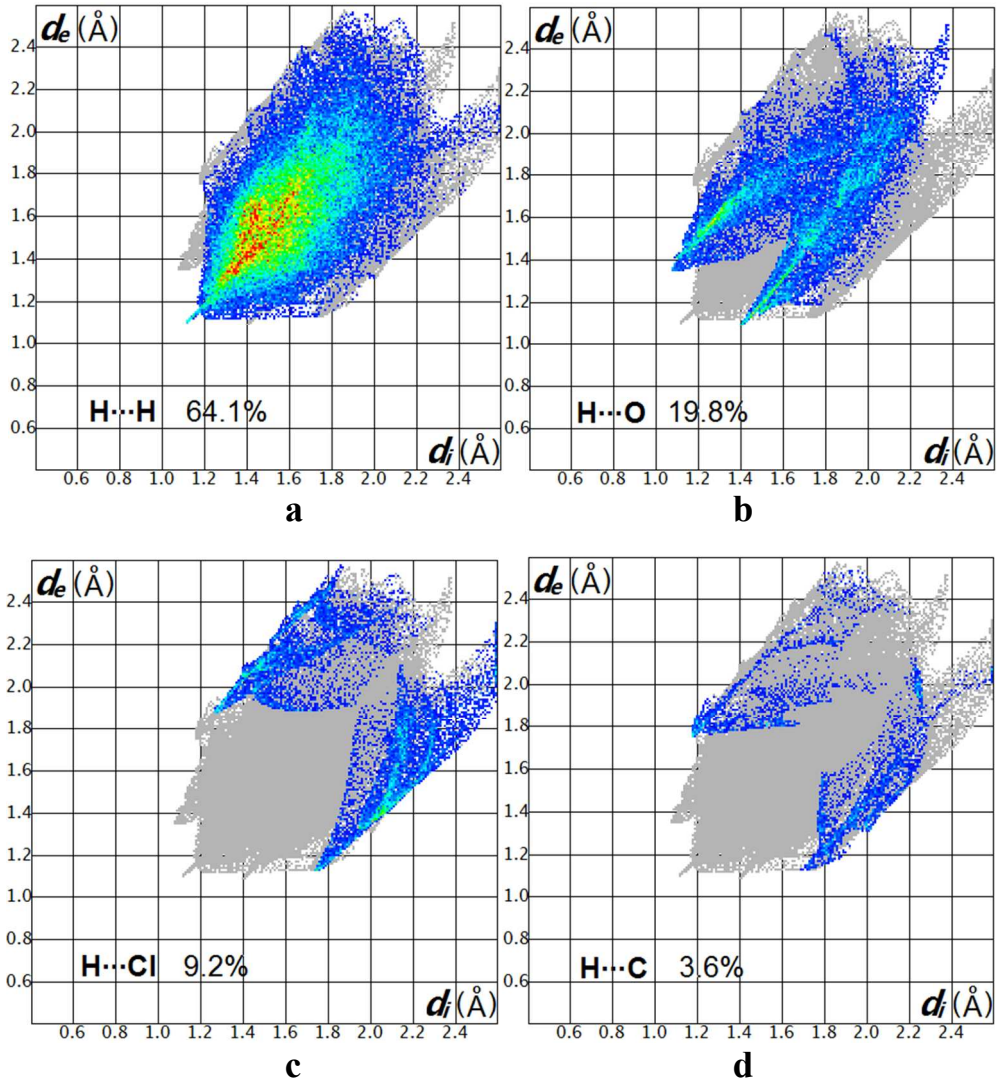

Figure 9. Fingerprint plots for **I** resolved into (a) H···H, (b) H···O, (c) H···Cl and (d) H···C intermolecular contacts. The full fingerprint appears beneath each decomposed plots as a gray shadow.

From this analysis, emerges that the H···H interactions are the main contributions to the Hirshfeld surface area (64.1%). The relative contributions due to H···O, H···Cl and H···C contacts of molecule IA of **I** are 19.8, 9.3 and 3.6%, respectively. The smallest fingerprint contributions occur for Cl···O (2.2%), C···O (0.6%), Cl···C (0.3%) and O···O (0.2%).

In order to understand the nature of this intermolecular interactions, in addition to the Hirshfeld study a topological description of these contacts have been provided through the Bader´s AIM analysis at the M06-2X/6-31G(d,p) level of theory. Figure 10 shows the atomic interaction lines

(AIL´s) and bcp´s between all pairs of interacting atoms founded by AIM for a chosen tetramer. A total of 31 intermolecular bond critical points (*i-bcps*) are located in the region between the steroid units (Figure10b), corroborating the existence of the H···H, H···O, H···Cl, H···C and Cl···O intermolecular interactions previously determined by the Hirshfeld surface tools. From the AIM analysis a total of sixteen H···H (51.6 %), eight H···O (25.8 %), three H···Cl (9.7 %), two H···C (6.4 %) and two Cl···O (6.4 %) *i-bcps* were obtained. The selected tetramer reproduces the behavior of the entire crystallographic cell, being the H···H contact the most important contribution to the crystal packing of **I**, as from the Hirshfeld analysis (Figure 9a). We were unable to locate AIL´s and bcp´s for the C···O, Cl···C, and O···O intermolecular contacts for the tetramer unit, as obtained from the Hirshfeld analysis.

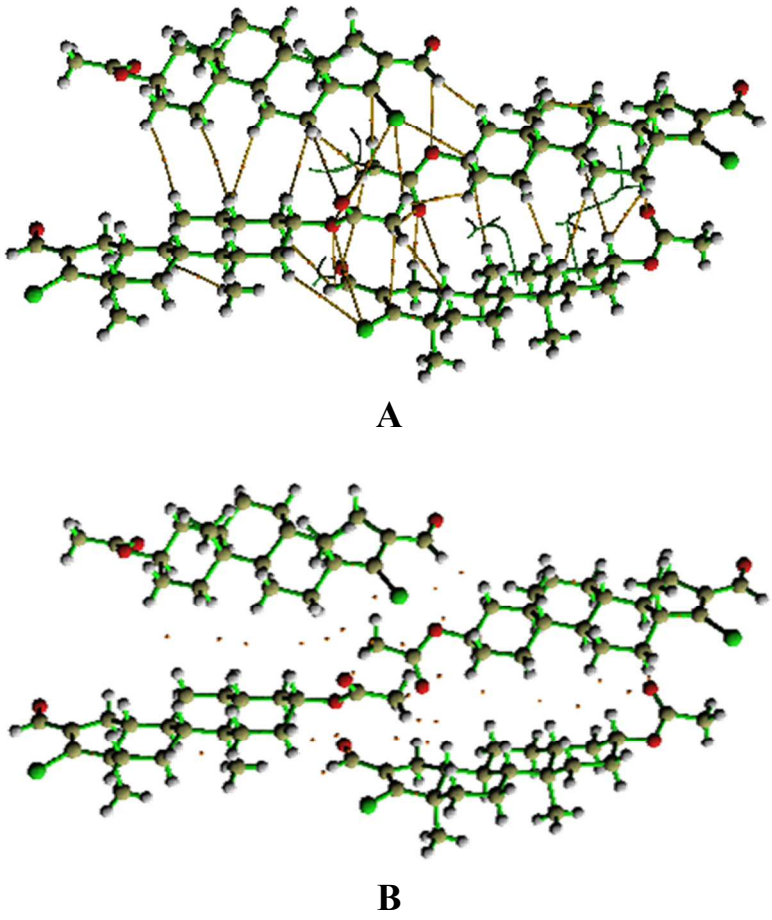

Figure 10. Structures of the stationary point of a tetramer unit at M06-2X/6-31G(d,p) level of theory. (a) Atomic interaction line (AIL) in brown color, and bond critical points as yellow circles.(b) Same representation without the AIL.

Table 3 shows the values of four local parameters: the electron density ρ(bcp), the Laplacian of the electron density $\nabla^2\rho(bcp)$, the kinetic energy density G_{bcp} and the potential energy density V_{bcp} at the bond critical point of the most important intermolecular interactions. The AIM analysis was performed at the M06-2X/6-31G(d,p) level of theory. Figure 11 presents the contour line maps of the Laplacian of ρ characterizing each of these intermolecular interactions.

Table 3. Topological properties of the bond critical points (bcp) with topology (3;-1) for the intermolecular interactions in the tetramer unit at the M06-2X/6-31G(d,p) level of theory.

Intermolecular X…Y Interaction	D(X…Y) (Å)	ρ(bcp)	$\nabla^2\rho(bcp)$	$\left(\frac{\lvert V_{bcp}\rvert}{G_{bcp}}\right)$	H(bcp)
H17A···H4D	2.547	0.003	0.013	0.631	0.00090
H5A···H1D	2.440	0.004	0.014	0.691	0.00084
H2A···H7D	2.917	0.002	0.006	0.659	0.00035
H15A···O2B	2.508	0.009	0.034	0.834	0.00122
H14A···O2B	2.639	0.007	0.026	0.817	0.00101
H22E···O2B	2.738	0.006	0.021	0.785	0.00092
H22D···Cl1A	2.980	0.005	0.019	0.663	0.00120
H2E···Cl1A	3.477	0.002	0.007	0.657	0.00042
H22E···C18A	3.356	0.003	0.008	0.695	0.00045
Cl1A···O2B	3.743	0.003	0.012	0.697	0.00068

X and Y- atoms involved in the intermolecular interaction. Units of ρ, $\nabla^2\rho(bcp)$and H(bcp) in a.u.

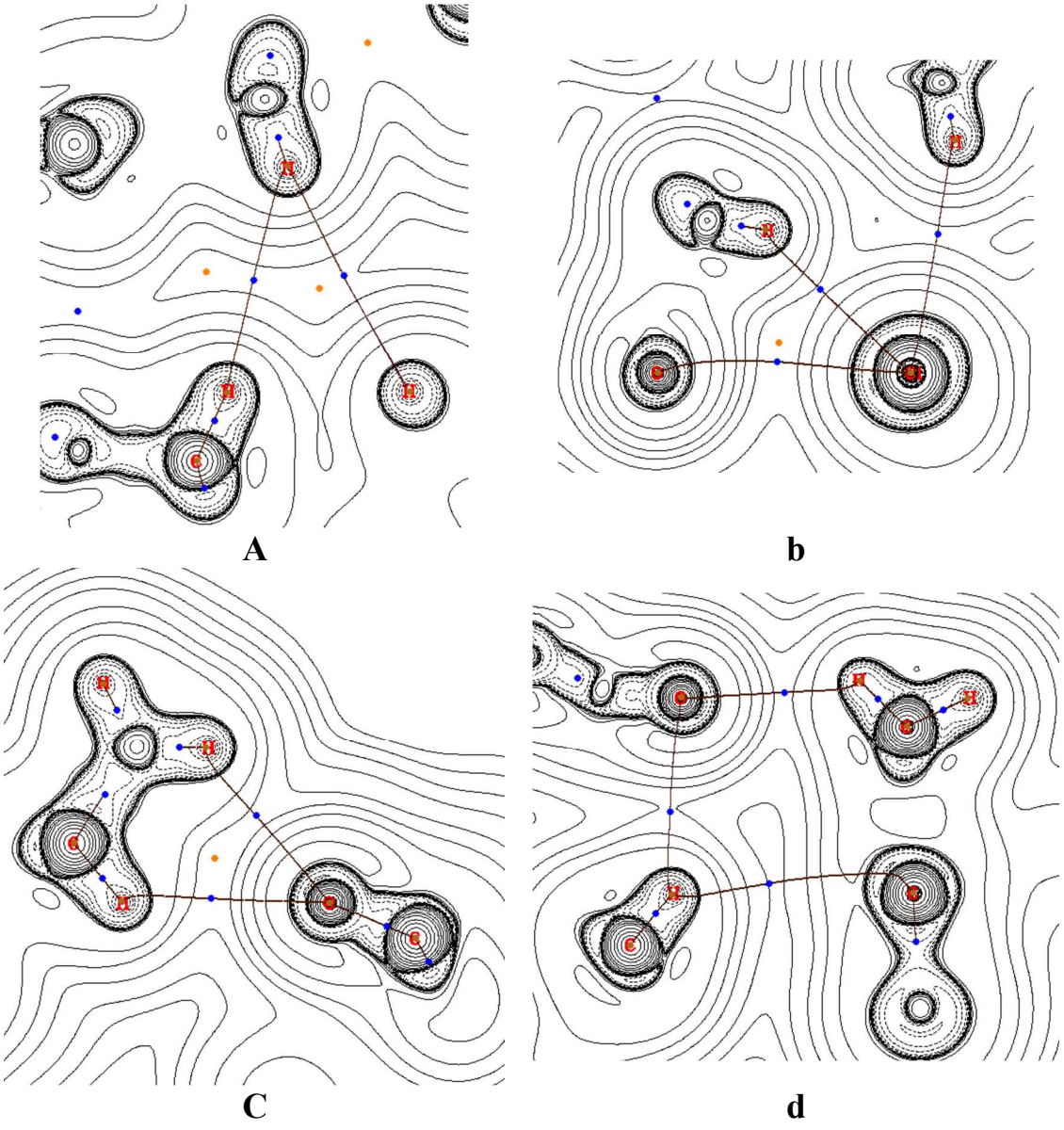

Figure 11. Contour line map of the Laplacian of ρ for (a) H···H, (b) H···Cl and Cl···O (c) H···O, (d) H···C intermolecular interactions in the tetramer unit at the M06-2X/6-31G(d,p) level of theory. Blue circles represents bond critical points (3;-1), yellow circles represents ring critical points (3;+1).

As can be seen, the ρ(bcp) is in the known range (0.002-0.035 a.u.) for all the studied *i-bcps* (Table 3) to be properly considered as closed-shell interactions. In addition, excluding the *i-bcps* presented among the H2A···H7D, H2E···Cl1A, H22E···C18A and Cl1A···O2B interactions, the $\nabla^2\rho(bcp)$ is in the recognized range (0.014-0.139 a.u.) for non-covalent interactions. It is well-

known that closed-shell interactions involve different types of bonding as for example vdW, ionic, and hydrogen bonding interactions. Although the interactions mentioned before show the $\nabla^2\rho(bcp)$ out of the 0.014-0.139 a.u. range to be considered as closed-shell interaction type, all these intermolecular contacts show a positive sign of the Laplacian, which is an important criteria to be classified as non-covalent interactions. Moreover, H2A···H7D, H2E···Cl1A, H22E···C18A and Cl1A···O2B show the lowest ρ(bcp) and $\nabla^2\rho(bcp)$ values, and therefore can be considered as weak vdW interactions. This was expected, since for these cases the D(X···Y) distance is near or greater than 3 Å, which is a typical vdW distance.[56]

It is common to use the ρ(bcp) as a direct measure of the strength of a non-covalent interaction,[57] then in our case the H···O intermolecular interactions show the greatest values of ρ(bcp) and $\nabla^2\rho(bcp)$, which indicates a greater strength of these interactions as compared to the rest in Table 3. The H15A···O2B possess the highest strength of all the analyzed intermolecular interactions presented in this tetramer unit. This result is in agreement with the Hirshfeld fingerprint plots and geometrical Jeffrey´s criteria[55] (Figure 9b), which define this interaction as a strong H···O intermolecular contact, [H15A···O2B^{i} = 2.508(2) Å, (i) 1+x, y,z]. According to ρ(bcp) and $\nabla^2\rho(bcp)$ values, the strongest intermolecular interactions of this particular tetramer are the H···O followed by H22D···Cl1A, H···H, Cl···O and C···H. Closed-shell interactions such as vdW and hydrogen bonds are characterized by |V(bcp)|/G(bcp) ratio lower than 1 and positive $\nabla^2\rho(bcp)$ and electronic energy density (H(bcp)) values.[58] In our studied intermolecular contacts (Table 3), the |V(bcp)|/G(bcp) is always lower than 1 and H(bcp)>0, which shows the domination of kinetic energy density G(bcp) over the potential energy density V(bcp) that characterizes closed-shell interactions. The O···H and H22D···Cl1A interactions possess the highest |V(bcp)|/G(bcp) values and most positive H(bcp) which allows to classify them as moderate

hydrogen bonds, while H2E···Cl1A, H···H, C···H and Cl···O contacts can be classified as weak closed-shell vdW interactions.

Figure 12 maps the ρ(r)*signλ_2 quantity onto the RDG isosurfaces and allows to qualitatively reveal both the nature and strengths of the interactions.[59-61] The λ_2 is the second eigenvalue ($\nabla^2\rho = \lambda_1 + \lambda_2 + \lambda_3$) of the electron density Hessian matrix. This map shows a continuous color code scheme based on the second derivative sign (sign λ_2), where strong attractive interactions are presented in blue (ρ(r)*signλ_2<0), weak interactions in green (ρ(r)*signλ_2≈0) and strong repulsive interactions in red (ρ(r)*signλ_2<0).[59] The four steroid molecules representing the chosen tetramer unit are separated by van der Waals interaction regions. The green filled-color or light brown means that the electron density is low and characteristic of weak vdW interactions where ρ(r)*sign λ_2≈0. Obviously, the red regions correspond to the strong steric effects in the steroidal rings. Overall, these vdW interactions represent the most important contributions to the stability of this tetramer unit, as predicted by the AIM method.

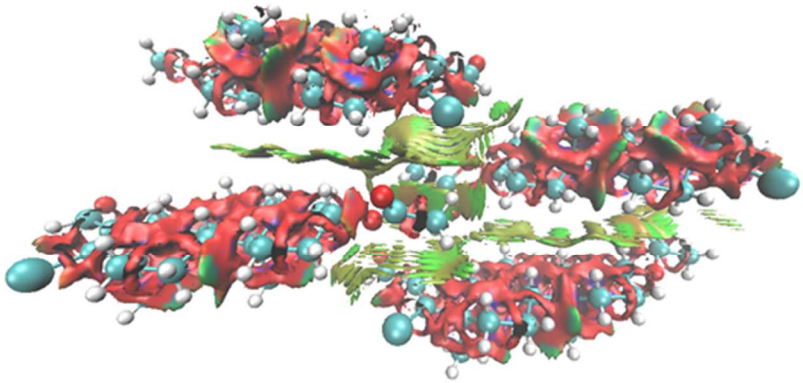

Figure 12. Gradient isosurfaces (s=0.5 a.u.) for the model tetramer unit at the M06-2X/6-31G(d,p). The surfaces are colored on a blue-green-red scale from -0.05<sign(λ_2)ρ(r)<+0.05 a.u.

CONCLUSIONS

The molecular structure of the 3β-acetoxy-17-chloro-16-formyl-5α-androstan-16-ene (**I**) has been determined by single-crystal X-ray diffraction. The X-ray data reveal that it crystallizes with three

independent molecules in the asymmetric unit, all of them with a similar conformation. An excellent agreement has been obtained between the M06-2X/6-311++G(d,p) optimized geometry and the IB crystallographic independent molecule. AIM and NBO analyses of the steroid molecule revealed that the conformer with hydrogen and chlorine atoms in syn disposition is mainly stabilized by three NBO contributions in the following order of importance: $\pi_{C=C}$-$\pi^*_{C=O}$ > $\pi_{C=O}$-$\pi^*_{C=C}$ > $n^{(\pi)}_{Cl}$ -σ^*_{C18-H}. The shape of the double well potential is related with two most significant contributions, the $\pi_{C=C}$-$\pi^*_{C=O}$ orbitals interaction and also to Pauli repulsion effects. The intra- and intermolecular interactions responsible for the crystal packing of this steroidal molecule were theoretically studied by both AIM and NBO methods, revealing the formation of the C-H···Cl intramolecular hydrogen bond. The stability of the crystal structure is mainly due to weak H···H, H···Cl and H···C van der Waals contacts and also to moderate intermolecular O···H hydrogen bond interactions. The H···H interactions possess the greatest contributions to the Hirshfeld surface area. Both intra and intermolecular contacts show the importance of non-classical hydrogen bonds interactions in establishing the organization of the extended structure.

Experimental

Crystal structure determination

Recrystallization of 3β-acetoxy-17-chloro-16-formyl-5α-androstan-16-ene (**I**) from methanol at room temperature gave colorless single crystals suitable for X-ray analysis.

Single crystal X-ray data were collected on a Enraf-Nonius CCD diffractometer[62] using monochromat dMoK α radiation (λ = 0.71073 Å) up to $2\theta_{max}$of 54.2° at room temperature. The structure was solved using direct and conventional Fourier methods with SHELXS.[63] and refined by full-matrix least-squares techniques based on F^2 using SHELXL.[63] All non-hydrogen atoms

were refined anisotropically; hydrogen atoms were located from difference Fourier maps and refined at idealized positions with a 'riding model'. Further details concerning data collection and refinement data are given in Table 4. The geometry of the molecule was calculated using the WinGX[64] and PARST[65] softwares. ORTEP-3[66] and MERCURY[67] programs were used for the molecular graphics. Crystal Explorer 3.0 program[68] for calculation and display of Hirshfeld surfaces and 2D fingerprint plots for the IA molecule was used, since there is no significant differences in the relative contributions to the Hirshfeld surface area for the intermolecular contacts of the three molecules in compound **I** (Table S6, Supporting Information). These 2D plots are derived from the Hirshfeld surface by plotting the fraction of points on the surface as a function of the pair (di, de). The points on the 2D graph represent a pair formed by discrete intervals (0.01 x 0.01 Å) of di and de. The fractions of surface points are codified by colors in the range from blue (relatively low fraction) through green (moderate fraction) to red (highest fraction). The (de + di) value represent the approximated intermolecular distance corresponding to a particular interaction.[54]

Table 4. Crystal data and structure refinement for compound **I**

Empirical formula	$C_{22}H_{31}ClO_3$
Formula weight	378.92
Temperature (K)	293(2)
Wavelength (Å)	0.71073
Crystal system	Orthorhombic
Space group	$P2_12_12_1$
Unit cell dimensions	
a (Å)	7.482(1)
b (Å)	22.751(1)
c (Å)	36.294(1)
α (°)	90
β (°)	90
γ (°)	90
Volume (Å^3)	6178.1(1)
Z	12
Density (calculated), Mg/m^3	1.222
Absorption coefficient, mm^{-1}	0.204
F(000)	2448
Crystal size (mm)	0.24 x 0.18 x 0.15
Theta range for data collection	3.45 to 27.10
Index ranges	$0 \le h \le 9$, $0 \le k \le 29$, $0 \le l \le 46$
Reflections collected	7356
Independent reflections	7356 [R(int) = 0.0374]
Data/restraints/parameters	7356 / 0 / 724
Goodness-of-fit on F^2	1.027
Final R indices [(I)>2θ(I)]	R1 = 0.0484, wR2 = 0.1093
R indices (all data)	R1 = 0.0669, wR2 = 0.1202
Largest diff. peak and hole (e/A^{-3})	0.174 and -0.230
Absolute structure parameter[69]	0.56(7)

Computational details

C-H···Cl intramolecular interaction

A relaxed potential energy scan by using M06-2X/6-31++G(d,p)[70] was performed to a small model of compound **I**. The aim of this scan was to analyze the presence of the intramolecular C-H···Cl interaction, this model only contains the *C* and *D* rings of this steroid. The torsion angle C17-C16-C18-H was varied from 0 to 360° with a grid size of 30°. Density critical point analyses on the model compound at the M06-2X/6-311++G(d,p) level of theory were carried out by using the Bader's atoms in molecule analysis (AIM).[19]

After the energy profile of this restricted model was obtained, a constrained optimization was performed to the geometry of compound **I** at specific values of the C17-C16-C18-H scanned torsion angle (0°, 90° and 180°) by using the same level of theory, e.g. M06-2X/6-31++G(d,p). Electron localization function (ELF)[33] of conformers with 0° and 180° were obtained at the M06-2X/6-31++G(d,p) level of theory. In addition, the obtained global minimum energy geometry of this compound was re-optimized at the M06-2X/6-311++G(d,p). Frequency calculations were also performed to ensure the presence of minima energy conformers. The natural bond orbital (NBO)[21] analysis was also employed to study the intramolecular orbital interactions in the stationary points of compound **I**.

Intermolecular interactions

Intermolecular interactions between the steroid units of the unit cell were characterized by means of the AIM analysis,[19] and only four units (e.g. a tetramer) from the CIF file were taken. The M06-2X/6-31G(d,p) level of theory was used considering the size of the entire crystallographic cell, and the high computational cost that requires taking into account all the system at the same level of theory. In addition, this tetramer represents the main intermolecular interactions among the steroid units.

All Density Functional Theory (DFT) calculations have been performed with the Gaussian09 package.[71] The Multiwfn package program[72] was employed for visualizing the ELF contour maps, the bond paths and to calculate the bond critical points. Also, this program has been used to obtain the Reduced Density Gradient (RDG) function, which represents a fundamental dimensionless quantity coming from the density and its first derivative.[73] In order to visualize the position and nature of non-covalent interactions in 3D space,[58-60] the gradient isosurfaces (s=0.5 a.u.) of the RDG at low densities, colored on a blue-green-red scale according to values of sign $(\lambda_2)\rho(r)$, and ranging from -0.05 to 0.05 a.u were obtained.

For statistical comparisons of geometrical parameters both the mean deviations (*MD*) and the ratio among experimental and theoretical parameters *r(exp/theor)* were used.

Supporting Information

Tables S1-S6 contains the complete experimental and theoretical structural data and mean deviation values are presented in Figure S1. Detailed crystallographic data have been deposited at the Cambridge Crystallographic Data Centre (CCDC-925060) and are available on request. These data can be obtained free of charge via www.ccdc.cam.ac.uk/data_request/cif, or by e-mailing data_request@ccdc.cam.ac.uk, or by contacting The Cambridge Crystallographic Data Centre, 12 Union Road, Cambridge CB2 1EZ, UK; fax: +44(0)1223-336033.

Acknowledgments

Financial support by the Ministerio de Ciencia e Innovación (MINECO) of Spain (CTQ2011-24652) is acknowledged. H. P. thanks financial support from Ph.D. Cooperative Program-ICTP/CLAF.

References

1. G. Mehta and V. Singh, *Chem. Soc. Rev.*, 2002, **31**, 324–334.

2. H. Guo, H. Wu, J. Yang, Y. Xiao, H. J. Altenbach, G. Qiu, H. Hu, Z. Wu, X. He, D. Zhou and X. Hu, *Steroids,* 2011, **76**, 709-772.

3. V. M. Moreira, J. A. R. Salvador, A. M. Bejad and J. A. Paixaod, *Steroids*, 2011, **76**, 582-587.

4. C. M. Marson, *Tetrahedron*, 1992, **48**, 3659-3726.

5. Shamsuzzaman, H. Khanam, A. Mashrai and N. Siddiqui. *Tetrahedron Lett*., 2013, **54**, 874-877.

6. D. P. Jindal and D Pathak, *Eur. J. Med. Chem.,* 1991, **26**, 651-654.

7. M. Shaheon-Khan, Z. Tabassum and M. Alain, *Indian J. Chem.*, 2009, **48B**, 1183-1186.

8. A. I. Siddiqui, V. U. M. Rao, M. A. Maimiraini and H. Siddiqui, *J. Heterocycl. Chem.*, 1995, **32**, 353-354.

9. R. Soiaky and C. Pallini, *Tetrahedron Lett.,* 1964, **28**, 1839-1845.

10. R. Sciaky and F. Mancini, *Tetrahedron Lett.,* 1965, **2**, 137-142.

11. M. J. Grimwade and M. G. Lester, *Tetrahedron,* 1969, **25**, 4535-4541.

12. A. Ruiz, J. Coro, L. Almagro, J. A. Ruiz, D. Molero, E. E. Maroto, S. Filippone, M. A. Herranz, R. Martínez-Álvarez, J. C. Sancho-García, F. Di Meo, M. Suárez and N. Martín, *J. Org. Chem.*, 2013, **78**, 2819-2826.

13. R. M. A. Pinto, J. A. R. Salvador and J. A. Paixão, *Acta Cryst.,* 2008, **C64**, o279-o282.

14. M. Soriano-García, T. Segura, N. Valencia, E. Bratoeff and M. Cabeza, *J. Chem. Crystallogr.,* 2010, **40**, 1119-1124.

15. L. C. R. Andrade, J. A. Paixão, M. J. M. de Almeida, F. M. Fernandes Roleira and E. J. Tavares da Silva, *Acta Cryst*., 2005, **C61**, o131-o133.

16. L. C. R. Andrade, J. A. Paixão, M. J. M. de Almeida, E. J. Tavares da Silva and F. M. Fernandes Roleira, *Acta Cryst*., 2005, **E61**, o1144-o1146.

17. L. C. R. Andrade, M. J. B.M. de Almeida, J. A. Paixão, J. F. S. Carvalho and M. L. Sá e Melo, *Acta Cryst.,* 2011, E67, o1056-o1057.

18. L. C. R. Andrade, J. A. Paixão, M. J. M. de Almeida, F. M. Fernandes Roleira and E. J. Tavares da Silva, *Acta Cryst*., 2009, **E65**, o814.

19. R. F. W. Bader, *J. Chem. Phys*., 1980, **73**, 2871-2883.

20. R.F.W Bader, *Acc. Chem. Res.,* 1985, **18**, 9-15.

21. A. E. Reed, L. A. Curtiss and F. Weinhold, *Chem. Rev*., 1988, **88**, 899-926.

22. D. Cremer and J. A. Pople, *J. Am. Chem. Soc*., 1975, **97**, 1354-1358.

23. M. Ramos-Silva, V. M. Moreira, C. Cardoso, A. Matos-Beja and J. A. R Salvador, *Acta Cryst. C*, 2008, **64**, o529-o531.

24. S. T. Rao, E. Westhof and M. Sundaralingam, *Acta Cryst. A,* 1981, **A37**, 421-425.

25. M. R. Caira, J. K. Guillory and L. Ch. Chang, *J. Chem. Crystallogr.,* 1995, **25**, 393-400.

26. M. Soriano-García, T. Segura, N. Valencia, E. Bratoeff and M. Cabeza, *J. Chem. Crystallogr*., 2010, **40**, 1119-1124.

27. F. H. Allen, O. Kennard, D. G. Watson, L. Brammer, A. G. Orpen and R. Taylor, *J. Chem. Soc*. *Perkin 2,* 1987, S1-S9.

28. E. A. Zhurova, V. V. Zhurov, D. Chopra, A. I. Stash and A. A. Pinkerton, *J. Am. Chem. Soc.,* 2009, **131**, 17260-17269.

29. D. Parrish, E. A. Zhurova, K. Kirschbaum, A. A. Pinkerton, *J. Phys. Chem. B.,* 2006, **110**, 26442-26447.

30. E. A. Zhurova, C. F. Matta, N. Wu, V. V. Zhurov and A. A. Pinkerton, *J. Am. Chem. Soc.,* 2006, **128**, 8849-8861.

31. M. L. DeRider, S. J. Wilkens, M. J. Waddell, L. E. Bretscher, F. Weinhold, R. T. Raines and J. L. Markley, *J. Am. Chem. Soc*., 2002, **124**, 2497-2505.

32. R. R. Sauers, *Comp. Theor. Chem*., 2011, **970**, 73-78.

33. I. V. Alabugin, K. M. Gilmore and P. W. Peterson, *WIREs Comput. Mol. Sci.,* **2011**, *1*, 109–141.

34. M. Alecu, J. Zheng, Y. Zhao and D. G. Truhlar. *J. Chem. Theory Comput.,* **2010**, *6,* 2872-2887.

35. A. D. Becke and K. E. Edgecombe, *J. Chem. Phys.,* 1990, **92**, 5397-5403.

36. A. Mohajeri and E. Karimi, *J. Mol. Struct.: THEOCHEM*, 2006, **774**, 71-76.

37. H. Roohi, M. Habibi and M. Hasannejad, *Chem. Phys.,* 2006, **327**, 368-372.

38. I. Alkorta and J. Elguero, *Chem. Phys. Lett*., 2006, **417**, 367-370.

39. A. Nowroozia, H. Raissib and F. Farzad, *J. Mol. Struct.: THEOCHEM*, 2005, **730**, 161-169.

40. U. Koch and P. L. A. Popelier, *J. Phys. Chem.,* 1995, **99**, 9747-9754.

41. J. R. Lane, J. Contreras-García, J. P. Piquemal, B. J. Miller and H. G Kjaergaard, *J. Chem. Theory Comput.,* 2013, **9**, 3263-3266.

42. P. L. A. Popelier and R. F. W. Bader, *Chem. Phys. Lett*., 1992, **189**, 542-548.

43. K. Ponmalai and V. Nirmala, *J. Mol. Struct.,* 2004, **694**, 33-38.

44. P. L. A. Popelier, *J. Phys. Chem. A*, 1998, **102***,* 1873-1878.

45. A. H. Pakiari and S. Fakhraee, *J. Theor. Comput. Chem.,* 2006, **5**, 621-631.

46. G. R. Desiraju, *Acc. Chem. Res*., 2002, **35**, 565-573.

47. P.K. Thallapally and A. Nangia, *Cryst. Eng. Comm*., 2001, **27**, 1-6.

48. J. J. McKinnon, A. S. Mitchell and M. A. Spackman, *Chem. Eur. J.,* 1998, **4**, 2136-2141.

49. M. A. Spackman, *Phys. Scr.,* 2013, **87**, 048103, 12 pp.

50. J. J. McKinnon, D. Jayatilaka and M. A. Spackman, *Chem. Commun*., 2007, **37**, 3814-3816.

51. M. A. Spackman and D. Jayatilaka, *Cryst. Eng. Comm*., 2009, **11**, 19-32.

52. H. Pérez, R. S. Correa, A. M. Plutín, B. O'Reilly, M. B Andrade, *Acta Cryst*., 2012, **C68**, o19-o22.

53. S. L. Cuffini, J. F. Ellena, Y. P. Mascarenhas, A. P. Ayala, H. W. Sielser, J. M. Filho, G. A. Monti, V. Aiassa and N. R. Sperandeo, *Steroids*, 2007, **72**, 261–269.

54. J. J. McKinnon, F. P. A. Fabbiani and M. A. Spackman, *Cryst. Growth Design.,* 2007, **7**, 755-769.

55. G. A. Jeffrey, An Introduction to Hydrogen Bonding, Oxford University Press, Oxford, 1997.

56. K. Muller-Dethlefs and P. Hobza, *Chem. Rev.,* 2000, **100**, 143-167.

57. H. C. Suresh, N. Mohan, K. V. Neetha, K. Perya, R. George and J. M. Mathew, *J. Comput. Chem.,* 2009, **30**, 1392-1404.

58. S. J. Grabowski, *Chem. Rev*., 2011, **111**, 2597-2625.

59. E. R. Johnson, S. Keinan, P. Mori-Sánchez, A. Contreras-García, A. J. Cohen and W. Yang, *J. Am. Chem. Soc*., 2010, **132**, 6498-6506.

60. S. A. Vedha, R.V. Solomon, P. Venuvanalingam, *J. Phys Chem A.,* 2013, **117**, 3259-3538.

61. A. J. Cohen, P. Mori-Sánchez and W. Yang, *Science,* 2008, **321**, 792–794.

62. Enraf-Nonius 2000. *COLLECT*. Enraf-Nonius BV, Delft, The Netherlands.

63. G. M. Sheldrick, *Acta Cryst. A*., 2008, **64**, 112-122.

64. L. J. Farrugia, *J. Appl. Cryst.,* 1999, **32**, 837-838.

65. M. Nardelli, *J. Appl. Cryst*., 1995, **28**, 659.

66. L. J. Farrugia, *J. Appl. Cryst.,* 1997, **30**, 565.

67. C. F. Macrae, P. R. Edgington, P. McCabe, E. Pidcock, G. P. Shields, R. Taylor, M. Towler and J. van de Streek, *J. Appl. Cryst.,* 2006, **39**, 453-457.

68. S. K. Wolff, D. J. Grimwood, J. J. McKinnon, M. J. Turner, D. Jayatilaka and M. A. Spackman, Crystal Explorer (Version 3.0), University of Western Australia, 2012.

69. H. D Flack, *Acta Cryst. Section A,* 1983, **39**, 876-881.

70. Y. Zhao, D. G. Truhlar, *Theor. Chem. Acc*., 2008, **120**, 215-241.

71. M. J. Frisch, G. W. Trucks, H. B. Schlegel, G. E. Scuseria, M. A. Robb, J. R. Cheeseman, V. G. Zakrzewski, J. A. Montgomery, R. E. Stratmann, J. C. Burant, S. Dapprich, J. M. Millam, A. D. Daniels, K. N. Kudin, M. C. Strain, O. Farkas, J. Tomasi, V. Barone, M. Cossi, R. Cammi, B. Mennucci, C. Pomelli, C. Adamo, S. Clifford, J. Ochterski, G. A. Petersson, P.Y. Ayala, Q. Cui, K. Morokuma, D. K. Malick, A. D. Rabuck, K. Raghavachari, J. B. Foresman, J. Cioslowski, J. V. Ortiz, B. B. Stefanov, G. Liu, A. Liashenko, P. Piskorz, I. Komaromi, R.

Gomperts, R. L. Martin, D. J. Fox, T. Keith, M. A. Al-Laham, C. Y. Peng, A. Nanayakkara, C. González, M. Challacombe, P. M. W. Gill, B. Johnson, W. Chen, M. W. Wong, J. L. Andres, M. Head-Gordon, E. S. Replogle and J. A. Pople, Gaussian 03, Gaussian, Inc., Pittsburgh, PA, 1999.

72. T. A. Lu, Multifunctional Wavefunction Analyzer, Version 3.0. 2013. http://multiwfn.codeplex.com.

73. G. Saleh, C. Gatti and L. Lo Presti, *Comp. Theor. Chem*., 2012, **998**, 148-163.

Graphical Abstract